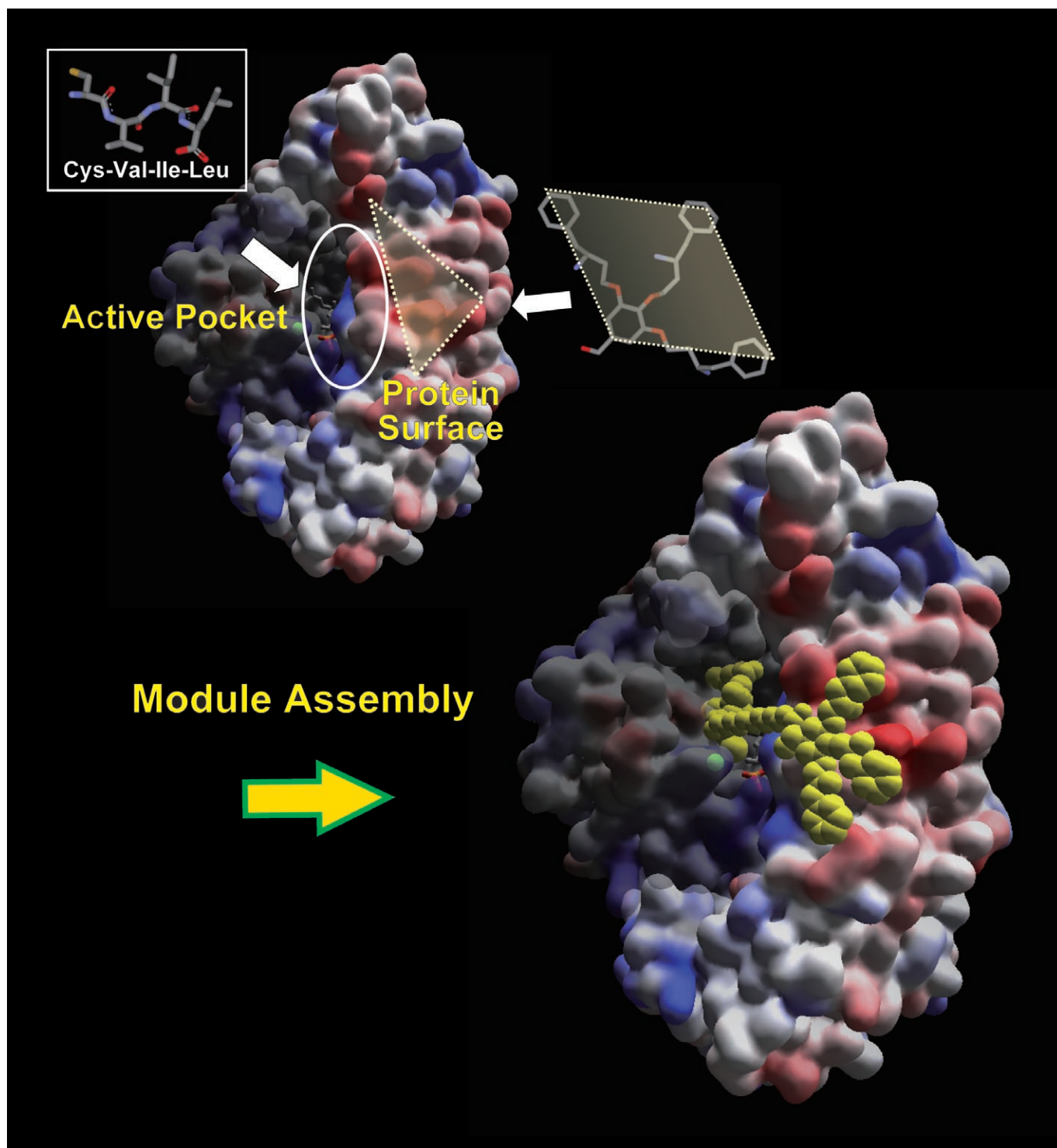# Module Assembly for Protein-Surface Recognition: Geranylgeranyltransferase I Bivalent Inhibitors for Simultaneous Targeting of Interior and Exterior Protein Surfaces

Shinnosuke Machida,[a] Kakeru Usuba,[b] Michelle A. Blaskovich,[c] Akiko Yano,[b] Kazuo Harada,[b] Saïd M. Sebti,[c] Nobuo Kato,[a] and Junko Ohkanda*[a]

Abstract: Synthetic chemical probes designed to simultaneously targeting multiple sites of protein surfaces are of interest owing to their potential application as site specific modulators of protein–protein interactions. A new approach toward bivalent inhibitors of mammalian type I geranylgeranyltransferase (GGTase I) based on module assembly for simultaneous recognition of both interior and exterior protein surfaces is reported. The inhibitors synthesized in this study consist of two modules linked by an alkyl spacer; one is the tetrapeptide CVIL module for binding to the interior protein surface (active pocket) and the other is a 3,4,5-alkoxy substituted benzoyl motif that contains three aminoalkyl groups designed to bind to the negatively charged protein exterior surface near the active site. The compounds were screened by two distinct enzyme inhibition assays based on fluorescence spectroscopy and incorporation of a [^{3}H]-labeled prenyl group onto a protein substrate. The bivalent inhibitors block GGTase I enzymatic activity with K_i values in the submicromolar range and are approximately one order of magnitude and more than 150 times more effective than the tetrapeptide CVIL and the methyl benzoate derivatives, respectively. The bivalent compounds **6** and **8** were shown to be competitive inhibitors, suggesting that the CVIL module anchors the whole molecule to the GGTase I active site and delivers the other module to the targeting protein surface. Thus, our module-assembly approach resulted in simultaneous multiple-site recognition, and as a consequence, synergetic inhibition of GGTase I activity, thereby providing a new approach in designing protein-surface-directed inhibitors for targeting protein–protein interactions.

Keywords: enzymes · GGTase I · inhibitors · proteins · proteomimetics

Introduction

Protein–protein interactions play a central role in numerous biological processes, including programmed cell death, proliferation and differentiation, and aging. In humans, roughly 40 000 to 200 000 protein interactions are estimated to exist.[1] Low-molecular-weight compounds that modulate such interactions in a selective manner are useful as probes to elucidate biological functions as well as drug leads for new therapeutic agents to target specific protein interfaces. Much effort has recently focused on the rational design of inhibitors based on proteomimetic strategies[2,3] to modulate protein–protein interactions, and a number of studies have been reported with success in this field.[4–6] For example, a general solution called "protein grafting" has been developed for transferring the functional epitope into a rigid miniature protein scaffold.[7,8] Similar approaches in combination with phase-display technique have also recently been developed with β-sheet templates[9,10] and β-hairpin cyclic peptidomimetics.[11]

Hamilton and co-workers used an elegant approach to create synthetic mimics of the antibody complementarity determining region (CDR) with nonpeptidic scaffolds, such as calixarenes[12,13] and porphyrins,[14–16] that accumulate multiple functional groups for targeting protein surfaces. These large synthetic antibody mimics were shown to require a large molecular surface for strong binding to the target. This approach demonstrated that the functionality of natural antibodies can be possibly mimicked by rationally designed synthetic molecules. However, in these examples, the molecular weight of the synthetic scaffold was still large. Increasing the binding affinity while decreasing the size of the molecule that is necessary for selective targeting is a challenging problem. To overcome this problem, we propose a strategy for protein-surface recognition that involves anchoring an exterior surface-binding module to an interior surface-binding module. The resulting bivalent compounds are expected to show increased affinity towards the target protein while leading to a decrease in the size of the protein-surface recognition scaffold required owing to a synergetic effect. One approach to test this hypothesis is the case of enzyme-inhibitor design in which a substrate mimic with high binding affinity and selectivity to the enzyme active site is linked to an exterior binding module that targets the appropriate sites on the protein surface. The resulting bivalent compounds are predicted to increase binding affinity (taking advantage of ΔG), and therefore the size of exterior binding module should decrease compared with that required for binding to the target by itself.

Strategies for bivalent or bisubstrate receptors have been utilized in recent chemical-biology studies, such as protein dimerization,[17,18] lead identification,[19] protein modifications,[20] and enzyme inhibitors.[21–30] Srivastava, Mallik, and co-workers have developed an efficient strategy to target the surface-exposed histidine side chains by using an imino-

[a] S. Machida, Prof. N. Kato, Prof. J. Ohkanda
The Institute of Scientific and Industrial Research (ISIR)
Osaka University, 8–1 Mihogaoka, Ibaraki, Osaka 567–0047 (Japan)
Fax: (+81) 6-6879-8474
E-mail: johkanda@sanken.osaka-u.ac.jp

[b] K. Usuba, A. Yano, Prof. K. Harada
Department of Life Sciences
Tokyo Gakugei University, Koganei, Tokyo 184–8501 (Japan)

[c] M. A. Blaskovich, Prof. S. M. Sebti
Drug Discovery Program at H. Lee Moffitt Cancer Center and Research Institute, Department of Molecular Medicine
University of South Florida, Tampa, FL 33612–9497 (USA)

Supporting information for this article is available on the WWW under http://www.chemeurj.org/ or from the author.

diacetate copper(II) complex.[24,31] In these examples, however, the motifs for the protein surface were designed for pinpoint binding of one or two amino acid side chains instead of targeting the large (≈ 1600 Å^2) surface areas that are typically involved in protein–protein interactions.[2–4] For modulating protein-surface functions, the anchoring strategy of a relatively large exterior binding motif with a smaller interior binding motif would provide a new approach for designing site-specific protein-surface receptors. As far as we are aware, there are no examples of nonpeptidic bivalent enzyme inhibitors that target the large protein surface areas that are involved in native protein–protein interactions.

Type I geranylgeranyltransferase (GGTase I)[32] is a heterodimeric zinc metalloenzyme and a member of the protein prenyltransferase family. This family of enzymes catalyzes the first step in a lipid post-translational modification that affects nearly 0.5% of cellular proteins.[33] Mammalian GGTase I is responsible for transferring a C20 geranylgeranyl group from geranylgeranyl pyrophosphate (GGPP) to a cysteine residue of the carboxy-terminus CAAX tetrapeptide of a target substrate protein; where C is cysteine, AA is an aliphatic dipeptide, and, in most cases, X is leucine or phenylalanine.[34] During the last decade, protein prenylation has become a major focus in anticancer research, and the major effort in developing prenyltransferase inhibitors focused on a related enzyme called farnesyltransferase (FTase). The aim was the specific inhibition of malignant transformation caused by mutated Ras and other farnesylated proteins.[35–37] The preclinical evaluation of FTase inhibitors was successful, with little toxicity, and several compounds are currently in clinical trials.[38]

Recently, GGTase I has been gaining much attention[39,40] owing to its potential to be a new target, not only for anticancer drugs,[41–45] but also for other diseases such as smooth muscle hyperplasia[46] and hepatitis C.[47] Its substrate proteins, such as RhoA,[48] RhoC,[49] Rac1,[50] Cdc42,[51] and RalA,[52] have been found to be implicated in promoting tumorigenesis and cancer metastasis. Very recently, a study using a GGTase I deficient mouse model has shown that GGTase I deficiency apparently improves the percentage of survival in mice with K-Ras-induced lung cancer, supporting the potential of GGTase I to be a clinical target.[44] A further significant observation that has been reported is that K-Ras4B, the most frequently mutated form of Ras in human tumors, becomes a substrate for GGTase I when FTase is blocked, and retains full biological activity.[53–55] As at least 5–10 times more proteins are geranylgeranylated than are farnesylated and the complex signaling pathways involving geranylgeranylated proteins have not been fully characterized, the development of potent and selective GGTase I inhibitors would provide useful tools for protein prenylation studies.

Mammalian GGTase I consists of a 48-kDa α subunit and a 43-kDa β subunit, which possesses the hydrophobic active pocket. The crystal structures of the ternary complex of GGTase I bound to the peptide and a GGPP analogue have revealed that there is a characteristic acidic region on the α-subunit protein surface near the entrance to the active pocket.[56–58] A number of studies have demonstrated that an unusual polylysine region near the carboxyl terminus of K-Ras4B is a critical determinant for geranylgeranylation catalyzed by GGTase I when FTase is inhibited.[59–62] Therefore, it is most likely that when the enzyme binds to K-Ras4B, the electrostatic attraction triggers the protein–protein interaction at the protein surface of GGTase I. In other words, GGTase I can be regarded as an enzyme that utilizes two distinct protein surfaces for substrate recognition in its native task, one is the interior surface of the substrate-binding cavity and the other is the protein exterior surface near the active site.

We therefore applied the concept of bivalent inhibitor design for simultaneous targeting of both surfaces of GGTase I (Figure 1). The interior surface-binding module
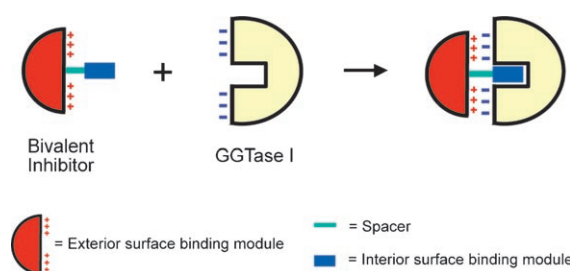

Figure 1. A schematic representation of the inhibitor design for simultaneous targeting of interior and exterior protein surfaces. Bivalent hybrid compound consist of an exterior surface-binding module (red) derived from a methyl gallate, an alkyl spacer (green), and an interior surface-binding module, Cys-Val-Ile-Leu-OH tetrapeptide.

(Figure 1, blue) should bind into the active pocket in a selective manner and should anchor the whole molecule near the pocket, whereas the exterior surface-binding module (Figure 1, red) requires relatively divergent structural features and multiple positively charged groups for the electrostatic interaction with the GGTase I surface. To explore the minimal and favorable distance in between the modules, we used different length spacers (Figure 1, green).

Herein, we describe the rational design of GGTase I bivalent inhibitors for simultaneous targeting of interior and exterior protein surfaces based on the module assembly strategy described in Figure 1.

Results and Discussion

Inhibitor design and chemistry: According to the GGTase I crystal structure, the substrate-binding pocket opens into the extensive α–β subunit interface and extends into the hydrophobic funnel-shaped cavity of the β subunit with an approximate inner diameter of 15 Å and a depth of 14 Å.[63] Near the entrance of the binding pocket, there is a characteristic cluster of acidic amino acid residues on the α-subunit protein surface where Glu125α, Glu160α, Glu161α, Glu187α, Asp191α, Glu229α, and Asp230α are located on
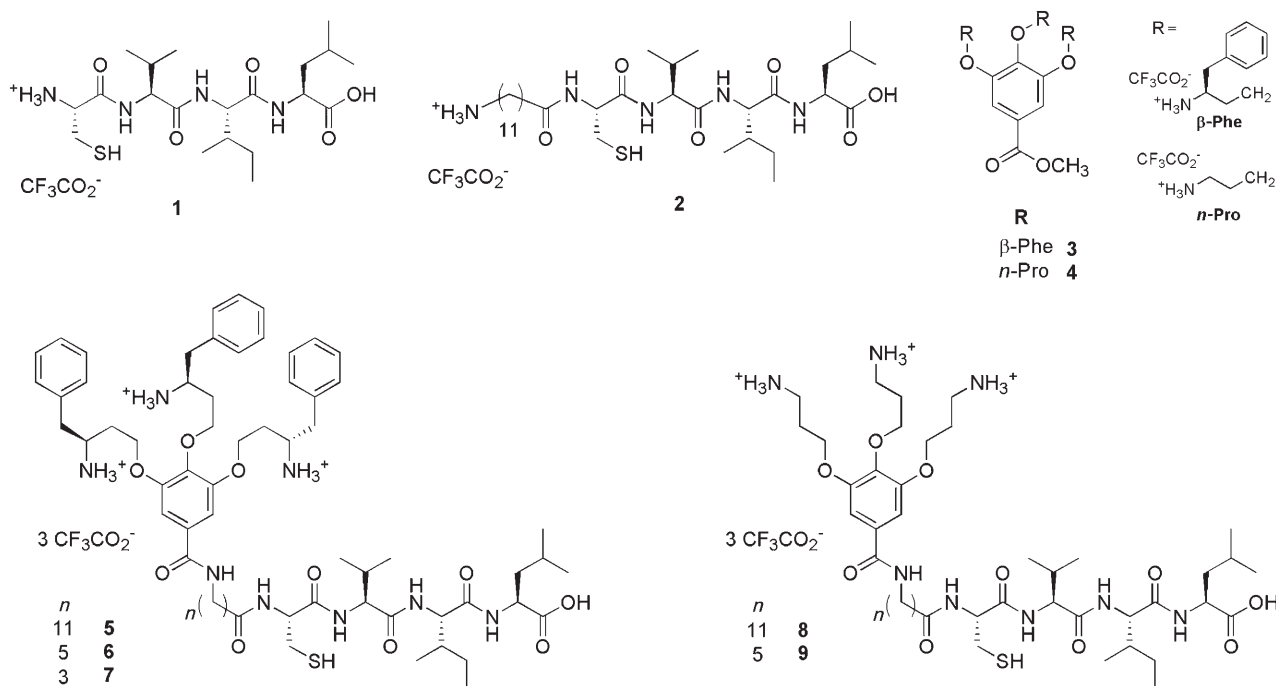
Scheme 1. Modules and hybridized compounds synthesized in this study.

the edge of the pocket lip. The compounds prepared on the basis of the design strategy are summarized in Scheme 1. For the interior surface binding module, Cys-Val-Ile-Leu-OH tetrapeptide (**1**), the CAAX sequence that is seen in GGTase I substrate proteins Rap-2b, and several others,[64] became our first choice because of its affinity to GGTase I with selectivity (IC$_{50}$/GGTase I = 2.3 μM; IC$_{50}$/FTase = 11 μM).[65] The size of the acidic surface of GGTase I is approximately 90 Å^2 and contains the seven acidic amino acid residues as well as several hydrophobic or neutral residues, such as Leu156α, Ala157α, Gln195α, and Asn194α. A molecular-modeling study showed that the methyl-3,4,5-trialkoxy-substituted benzoate derived from β-homophenylalanine derivative (**3**) possibly provides a complementary size (≈84 Å^2). In a further attempt to reduce the size of the exterior surface-binding module, *n*-propyl amine substituted derivative (**4**), in which three benzyl groups in **3** were removed, was also designed. These compounds were readily synthesized by alkylation of methyl gallate with the corresponding *N*-protected amino alkyl bromides, followed by deprotection (see the Supporting Information). These exterior surface-binding modules were attached to the N terminal of **1** by spacers of different lengths to give the bivalent hybrid compounds **5–9**.

To check whether the bivalent molecular sizes and shapes are relevant for the simultaneous two-site recognition, a superimposed model structure of **5** and GGTase I was built based on the previously reported X-ray crystal structure of the ternary complex of GGTase I[58] bound to a GGPP analogue and KKKSKTKCVIL. Within the complex, the portion of KKKSKTK was removed and the structure of **5** with-

out the CVIL moiety was installed. The resulting model showed that the trisubstituted benzoyl part provides an appropriate shape to bind the targeted acidic region of GGTase I (Figure 2).
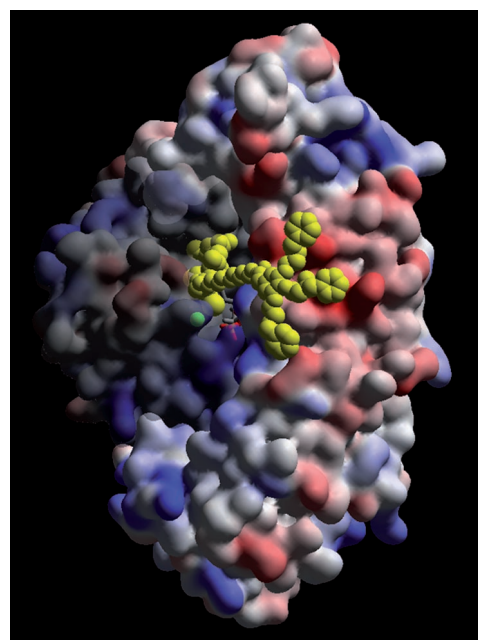

Figure 2. A superimposed model of **5** (yellow, CPK) and GGTase I crystal structure (PDB: 1N4Q). The catalytic Zn ion (green, CPK), GGPP analogue (stick); The bright area (right) and shadowed portions are the α and β subunits, respectively. Negatively charged and positively charged surfaces are shown in red and blue, respectively. DS Viewer 6.0.

Initial screening for inhibition activity by fluorescent enzyme assay: To examine whether the module-assembly approach results in bivalent inhibitors with better potency towards GGTase I, the compounds were initially screened at 5 μM for their ability to inhibit GGTase I in a fluorescent assay[66] by using geranylgeranyl pyrophosphate (GGPP; 5.0 μM) and the environmentally sensitive fluorogenic substrate, N-dansyl-Gly-Cys-Val-Ile-Leu-OH (DansGCVIL; 1.0 μM, $K_m = (0.28 \pm 0.04)$ μM; dansyl = 5-(dimethylamino)-naphthalene-1-sulfonyl; see Scheme S21 in the Supporting Information) in Tris-HCl buffer solution (Tris = tris(hydroxymethyl)aminomethane). This substrate increases the fluorescent intensity upon geranylgeranylation at the cysteine thiol group. Recombinant mammalian GGTase I was expressed and purified by a method previously reported.[67] The fluorescent increase was monitored for 5 min and the percentage of inhibition was calculated by comparison with the standard slope, which was taken from the reaction in the absence of inhibitors (see the inset in Figure 3A). The percentage of inhibition of GGTase I at a compound concentration of 5 μM is shown in Figure 3A. As expected, the various modules of the bivalent compounds were weak GGTase I inhibitors on their own. For example, CVIL (**1**), which has been shown to be a competitive inhibitor for GGTase I,[65] inhibited 42% of the enzyme activity (see the inset of Figure 3A); and compounds **2–4** inhibited the enzyme by 2–26%. However, the bivalent compound **6**, in which the modules **1** and **3** were hybridized, and compound **8**, in which modules **1** and **4** were linked, were both found to be more effective than either module alone and showed more than 87% inhibition. Concentration–response studies showed that the compound **6** inhibition curve is sigmoidal with an IC$_{50}$ value of 1.0 μM and a K_i of (0.22 ± 0.04) μM, both of which were calculated by using the Cheng–Prusoff equation (Figure 3B).[68] In contrast, the curves for the modules **1**, **2**, and **3** were apparently shifted to the higher concentration region. For example, the concentration required for 50% inhibition in the case of the tetrapeptide CVIL (**1**) was 6.9 μM, which was approximately seven times higher than that of **6**.

Concentration–response curves of the bivalent compounds (**5–7**) containing spacers of different lengths are summarized in Figure 4A. The results show that the spacer length affects the inhibitory activity of the bivalent compounds. Compound **7** ($n = 3$), which consists of a shorter spacer for the C2 unit than **6** ($n = 5$), was slightly less active than **6** ($K_i = (0.48 \pm 0.11)$ μM). On the other hand, compound **5** ($n = 11$), with a spacer length twice as long as that of **6** was less potent. This suggests that for compounds with the β-homophenylalanine type module, the longer spacers diminish the binding affinity to GGTase I owing to the entropical disadvantage.[69] However, as shown in Figure 4B, compound **8**, which has an equal length of spacer to that of **5** and a much simpler exterior module, restores the activity with a K_i value of (0.42 ± 0.09) μM. Elimination of the three benzyl groups from the exterior binding module in **5** should result in increased flexibility as well as decreased hydrophobicity around the three amino side chains of the benzoyl moiety in
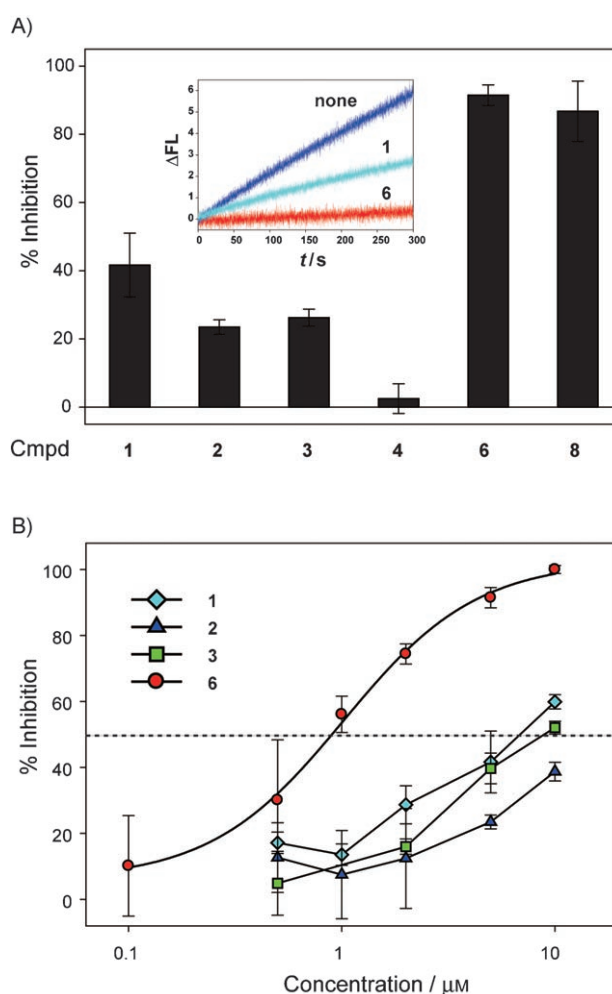

Figure 3. Fluorescent GGTase I inhibition assays were carried out by using GGPP (5 μM) and the fluorogenic substrate, DansGCVIL (1 μM) in 50 mM Tris-HCl, pH 7.5 at 30 °C. A) The results of primary screening of the % inhibition of GGTase I in the presence of 5 μM of module compounds (**1–4**) and the bivalent compounds (**6** and **8**). Inset: the time course fluorescence change at 520 nm (ex: 340 nm) in the absence of (blue) or in the presence of 5 μM of inhibitors (**1**, blue; **6**, red). The slopes were used for the calculations of percentage of inhibition. B) Concentration–response curves of the modules (**1**, **2**, and **3**) and the corresponding hybridized compound **6** plotted the % inhibition against the inhibitor concentrations. The IC$_{50}$ values were then used to calculate the inhibitory constants, K_i, by the Cheng–Prusoff equation (see reference [68]). The standard deviation is given for $n = 3$. δI_f = change in fluorescence intensity.

8 (calculated log P values: −0.9 for **3**, 5.08 for **4**).[70] Therefore, a possible explanation for the significant difference in the activity might be 1) with the long spacer ($n = 11$), the three 1-amino-1-benzyl-propyloxy groups in **5** do not take a suitable conformation for binding to the targeted surface owing to rigidity, whereas 1-amino-propyloxy groups are more flexible, thus the spacer length ($n = 11$) was able to deliver the moiety to the targeted site; or 2) the high hydrophobicity of **5** might result in random binding or possible aggregation. This observation prompted us to synthesize compound **9** in which the better aminopropyl module and the
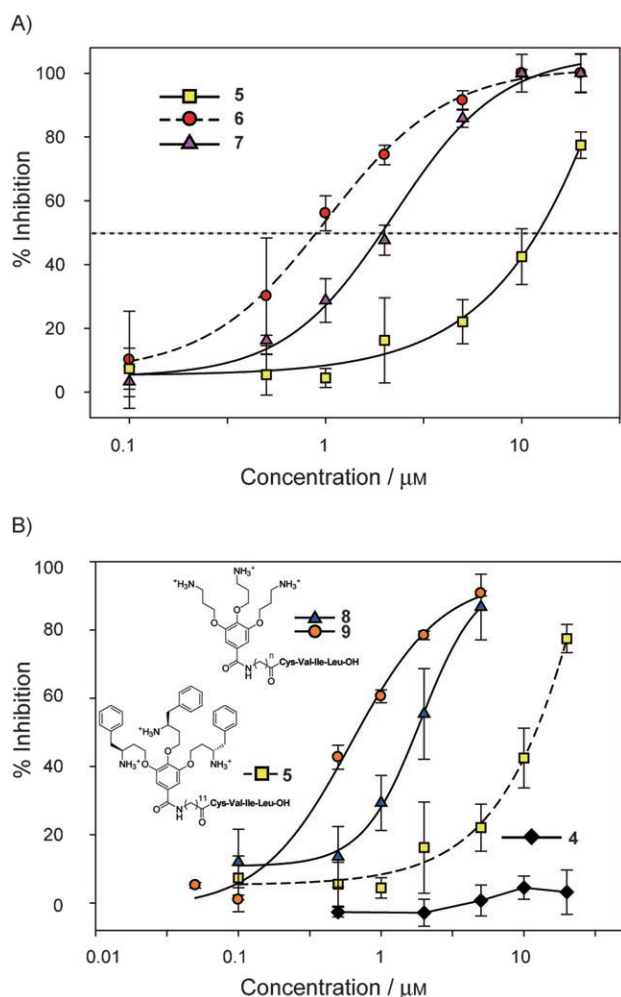
Figure 4. A) Dose–response curves for A) the bivalent compounds (**5**, **7**) with different a different spacer length than **6** and B) the methyl gallate derivative (**4**) compared with bivalent compound **8** and **9**, which consist of the methyl gallate as the exterior surface-binding module. The data set for **6** (A) and **5** (B) are shown for comparison (dashed line). The standard deviation values are given for $n=3$.

more widely used method, which measures the incorporation of [3H]GGPP and [3H]FPP (farnesylpyrophosphate) into the protein substrates, H-Ras-CVLL and H-Ras-CVLS, respectively, by using previously described methods.[71] The moderate inhibition activities against GGTase I of the tetrapeptides **1** and **2** were confirmed as shown in Table 1. No in-

Table 1. IC$_{50}$ values for inhibition of GGTase I and FTase in vitro by modules (**1–4**) and bivalent inhibitors (**5–8**).

| Cmpd | IC$_{50}$ [μM][a] | |
	GGTase I	FTase
1	4.8 ± 1.7	>100
2	1.4 ± 0.5	>100
3	>100	>100
4	>100	>100
5	0.98 ± 0.45	>100
6	0.64 ± 0.06	>100
7	0.66 ± 0.05	>100
8	0.60 ± 0.03	>100

[a] Where the standard deviation is given for $n=3$, or $n=1$.

hibition activity against FTase was detected with **1** or **2**, which is in agreement with the fact that CVIL is a selective inhibitor for GGTase I over FTase.[65] Neither benzoate derivative **3** nor **4** showed any activity. All the bivalent compounds (**5–8**) were confirmed to be potent for GGTase I with IC$_{50}$ values in the submicromolar range (Table 1) and most importantly, no inhibition was detected against FTase (IC$_{50}$: GGTase I/FTase >167 in the case of **8**). The selectivity observed here clearly indicates that the CVIL module in each bivalent compound recognizes and binds to the GGTase I active pocket but not to the FTase pocket. These results demonstrate that specificity is not compromised by our design strategy.

The spacer-length effect was also observed in this assay, showing that compounds **6** and **7** ($n=5$ and 3, respectively) were more potent (IC$_{50}=0.64$ and 0.66 μM, respectively) than compound **5** ($n=11$, IC$_{50}=0.98$ μM). It is noteworthy that compound **8**, a with smaller and less hydrophobic exterior binding module than **6**, was found to be equally effective with an IC$_{50}$ value of 0.60 μM, which was an improvement of eight times and greater than 167 times those of the corresponding modules, **1** and **4**, respectively. Again, these results confirmed that the molecular size of the hybrid inhibitors can be optimized by appropriately combining the modules.

Mode of inhibition: We next wanted to confirm that the inhibition mode of the bivalent inhibitor and the CVIL tetrapeptide was identical. To this end, Lineweaver–Burk analysis was carried out for peptide **1** and the bivalent compounds **6** and **8**. The data were analyzed by using equations for competitive, noncompetitive, and uncompetitive inhibition models. The data set for **1** clearly fit the competitive model (Figure 5A; $K_i=(0.97 \pm 0.19)$ μM). As shown in Figure 5B for **6**, these data also showed the best fit to the competitive model with an intersection point on the y axis ($K_i=$

optimal length of spacer ($n=5$) were combined. As shown in Figure 4B, **9** indeed showed improved activity compared with **8** with an IC$_{50}$ value of 0.62 μM and a K_i of (0.14 ± 0.03) μM, which has a similar activity to **6** and with a reduced molecular weight of 270. This suggests that the molecular size can be tuned by choosing 1) the minimal critical functional groups for the exterior binding module and 2) the most appropriate spacer length for the combination of modules. Notably, compound **4** showed no apparent inhibitory activity by itself (Figure 4B). The weak activity of modules **1** and **4**, and the synergistic effect seen with the bivalent inhibitor **9**, validates our module assembly approach that targets two critical sites on GGTase I.

Selectivity in GGTase I inhibition: To confirm the observation seen in the fluorescent assay and to evaluate the selectivity of our bivalent inhibitor for GGTase I over the related enzyme, FTase, we further tested the compounds (**1–8**) by a
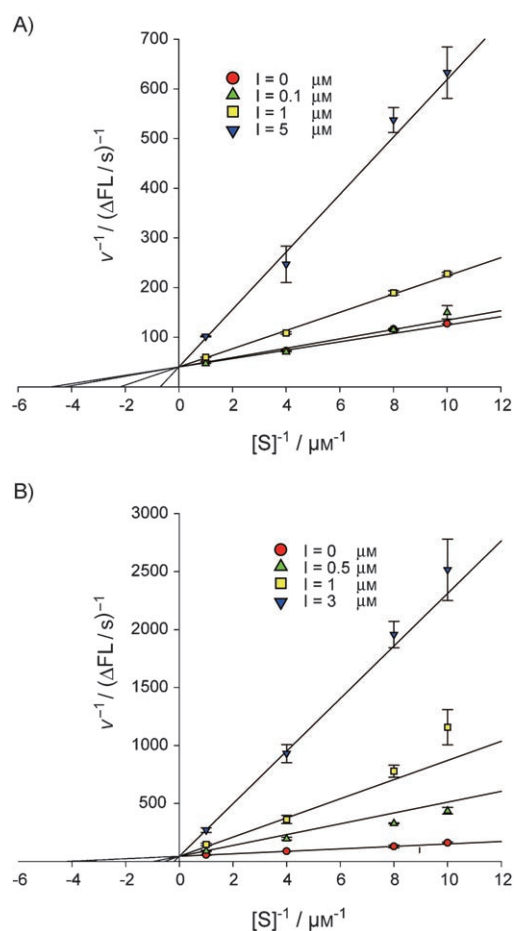
A)

B)

Figure 5. Kinetic analysis of the inhibition of GGTase I by CVIL tetrapeptide **1** and bivalent inhibitor **6**. GGTase I was treated with varying concentrations of A) the tetrapeptide **1** (0.1, 1, and 5 μM) and B) the bivalent compound **6** (0.5, 1, and 3 μM) with the substrate concentration increasing from 0.1 to 1 μM. [GGPP] = 5 μM, $T = 293$ K.

(0.15 ± 0.01) μM for **6** and (0.21 ± 0.03) μM for **8**; see Figure S2 in the Supporting Information for **8**).

As we used the native substrate peptide sequence for the interior surface binder, we wanted to clarify whether geranylgeranylation occurred on the thiol group of the bivalent compounds. The HPLC analysis showed that in the absence of inhibitor, the conversion of DansGCVIL to DansGC(GG)VIL was completed within 5 minutes (see Figure S3 A in the Supporting Information), whereas under the same conditions but in the presence of 20 μM **6**, the geranylgeranylation of DansGCVIL was completely suppressed (see Figure S3 B in the Supporting Information). Moreover, no change in the peak area of **6** nor new-product peak generation was detected for up to 50 minutes incubation with **6**, indicating that geranylgeranylation did not occur on the thiol group of **6** (see Figure S3 C in the Supporting Information). This is consistent with previous work with FTase in which some CAAX tetrapeptide mimetic inhibitors are not farnesylated. The crystal structural study has revealed that these FTase inhibitors bind in a distinct conformation from the substrate,[72] suggesting that the conformation in the

active-site-bound form is essential to dictate whether S-farnesylation occurs. Assuming that this is also the case in GGTase I, which is likely owing to its functional similarity, the binding of the exterior module to the protein surface may trigger structural changes of the interior binding module CVIL to avoid S-geranylgeranylation.

Conclusion

We have developed a new series of bivalent inhibitors for GGTase I based on a module assembly strategy for simultaneous targeting of interior and exterior protein surfaces. Coupling of CVIL tetrapeptide and a 3,4,5-trisubstituted benzoate derivative provided compounds **6** and **8** ($K_i = 0.15$ and 0.21 μM, respectively) and improved the inhibitory ability by approximately one order of magnitude and more than 150-fold compared with the corresponding modules. An explanation for the moderate additivity effect observed with the bivalent compounds compared with tetrapeptide **1** might be due to the remarkably weak affinity of the exterior binding modules **3** and **4**. All bivalent compounds were found to be highly selective for GGTase I over FTase (> 167 times). The spacer length was found to affect the potency, and very long spacers ($n = 11$) diminished the activity as seen in the case of **5**, which is consistent with a previous report.[69] Simply changing the exterior binder in **5** to one with less hydrophobic and more flexible side chains restored the activity, as seen in **8**. Thus, bivalent inhibitors targeting the exterior and the interior surfaces can be minimized by choosing the most appropriate modules and the spacer lengths. Interestingly, geranylgeranylation was not detected, at least in the case of **6**, suggesting that the exterior surface binding module may alter the CVIL conformation in the active pocket. Although it remains moderate, the synergetic inhibitory activity observed in this study strongly suggests that the exterior binding modules were specifically delivered to the targeted protein surface. Thus, we believe that the module-assembly strategy for designing bivalent protein inhibitors described herein provides a general strategy for specific targeting of the protein surface, which can be extended to other enzyme families for increased selectivity or for modulating protein–protein interactions.

We are currently extending this strategy to isozyme selective inhibitors and to dual inhibitors targeting characteristically distinct and identical protein-surface structures.

Experimental Section

spectrometer. Elemental analyses were performed on 2400CHN (Perkin Elmer).

Synthesis of 3,4,5-tris(3-amino-4-phenyl-1-butoxy)benzoic acid methyl ester trifluoroacetate (3): A solution of methyl gallate (101 mg, 0.549 mmol), [(1S)-3-bromo-1-(phenylmethyl)propyl]carbamic acid *tert*-butyl ester (**31**; 700 mg, 2.15 mmol; see the Supporting Information), potassium carbonate (444 mg, 3.21 mmol) in *N,N*-dimethylformamide (DMF; 20 mL) was stirred at 40°C for 24 h. After removal of DMF, the product was extracted with 10% CHCl$_3$ in AcOEt (600 mL) and 10% citric acid, and the organic layer was dried over Na$_2$SO$_4$. The crude product was purified by SiO$_2$ column chromatography (gradient from CHCl$_3$ alone, to CHCl$_3$:AcOEt = 1:1, and then to CHCl$_3$:MeOH = 50:1) to give 3,4,5-tris(3-*N*-(*tert*-butoxy)amino-4-phenyl-1-butoxy)benzoic acid methyl ester (**32**; see the Supporting Information) as a white solid (464 mg, 91%). m.p.: 167–168°C; ^{1}H NMR (400 MHz, CDCl$_3$): δ = 1.38 (m, 27H, Boc×3 (Boc = *tert*-butyloxycarbonyl), 1.82–2.10 (m, 6H, 3-, 4-, and 5-OCH$_2$CH$_2$), 2.77–2.87 (m, 6H, 3,4, 5-CH$_2$Ph), 3.88 (s, 3H, -OCH$_3$), 4.07–4.12 (m, 9H, 3,4,5-OCH$_2$CH$_2$CH), 4.69 (br s, 2H, 3- and 5-NH), 5.28 (br s, 1H, 4-NH) and 7.17–7.28 ppm (m, 17H, aryl H); HRMS–FAB (*m/z*): [M^++H] calcd for C$_{53}$H$_{72}$N$_3$O$_{11}$, 926.5167; found, 926.5152. Trifluoroacetic acid (TFA; 500 μL) in CH$_2$Cl$_2$ (500 μL) was added to a solution of **32** (25 mg, 27.0 μmol) and the mixture was stirred at 0°C for 1 h. After evaporation, Et$_2$O was added to the residue and the resulting white precipitate was collected by centrifugation to give compound **3** (30 mg, 100%). HPLC purity, 99%; ^{1}H NMR (400 MHz, CDCl$_3$): δ = 2.11–2.15 (m, 6H), 2.86 (m, 3H), 3.18 (m, 3H), 3.67 (m, 3H), 3.88 (s, 3H, OCH$_3$), 3.95 (s, 1H), 4.10 (s, 1H), 4.20 (s, 2H), 4.34 (s, 2H), 7.15–7.34 (m, 17H), 8.07–8.15 ppm (br s, 9H, NH$_3$); HRMS–FAB (*m/z*): [M^++H] calcd for C$_{38}$H$_{48}$N$_3$O$_5$, 626.3594; found, 626.3605.

Synthesis of *N*-[6-(3,4,5-tris(3-amino-4-phenyl-1-butoxy)benzoylamino)-hexylcarbonyl]-L-cisteinyl-L-valyl-L-isoleucyl-L-leucine trifluoroacetate (6): 1M KOH (1.3 mL, 1.3 mmol) was added to a solution of **32** (43 mg, 46.4 μmol) in CH$_2$Cl$_2$ (4 mL) and MeOH (8 mL) and the mixture was refluxed for 15.5 h. Evaporation, extraction with CHCl$_3$ (60 mL×3) and 10% citric acid (25 mL), and concentration gave the corresponding carboxylic acid (**33**, see the Supporting Information) as a white solid (43 mg, 100%). m.p.: 141–144°C; ^{1}H NMR (400 MHz, CDCl$_3$): δ = 1.38 (m, 27H, Boc×3), 1.82–2.05 (m, 6H, 3-, 4-, and 5-OCH$_2$CH$_2$), 2.80–2.87 (m, 6H, 3-, 4-, and 5-CH$_2$Ph), 4.09–4.13 (m, 9H, 3-, 4-, and 5-OCH$_2$CH$_2$CH), 4.69 (br s, 2H, 3 and 5-NH), 5.28 (br, 1H, 4-NH) and 7.17–7.28 ppm (m, 17H, aryl H); HRMS–FAB (*m/z*): [M^++H] calcd for C$_{52}$H$_{70}$N$_3$O$_{11}$, 912.5010; found, 912.4990. Benzotriazol-1-yloxytris(pyrrolidino)phosphonium hexafluorophosphate (PyBop; 67 mg, 0.13 mmol) in CH$_2$Cl$_2$ (1 mL) was added to a solution of **33** (90 mg, 98.7 μmol) and 6-aminohexanoic acid methyl ester hydrochloride (19 mg, 0.10 mmol), *N*-hydroxy-benzotriazole (HOBt; 31 mg, 0.20 mmol), and *N,N*-diisopropylethylamine (DIEA; 34 μL, 0.20 mmol) in DMF (5 mL) at 0°C and the mixture was stirred at RT for 13 h. After concentration, the product was extracted with CHCl$_3$ (200 mL), 10% citric acid, 5% NaHCO$_3$, and brine. The crude product was purified by SiO$_2$ column chromatography (CHCl$_3$/MeOH = 20:1) to afford the desired product (**35**; see the Supporting Information) as a white solid (101 mg, 98%). m.p.: 190–195°C; ^{1}H NMR (400 MHz, [D$_6$]DMSO): δ = 1.13–1.29 (m, 29H, 3-, 4-, and 5-Boc and -CH$_2$CH$_2$CH$_2$CO$_2$CH$_3$), 1.45–1.58 (m, 10H, -CH$_2$CH$_2$CO$_2$CH$_3$, -CONHCH$_2$CH$_2$ and 3-, 4-, 5-OCH$_2$CH$_2$), 1.77–1.90 (m, 6H, -OCH$_2$CH$_2$), 2.29 (t, *J* = 7.3 Hz, 2H, -CH$_2$CO$_2$CH$_3$), 2.66–2.78 (m, 6H, 3,4,5-CH$_2$Ph), 3.18–3.23 (m, 2H, -CONHCH$_2$), 3.56 (s, 3H, -CO$_2$CH$_3$), 3.83–3.99 (m, 9H, 3-, 4-, and 5-OCH$_2$CH$_2$CH), 6.55 (d, *J* = 8.3 Hz 1H, 4-NHBoc), 5.30 (d, *J* = 8.4 Hz, 2H, 3 and 5-NHBoc), 7.08 (s, 2H, benzoyl) 7.16–7.25 (m, 15H, 3-, 4-, and 5-Ph) and 8.33 ppm (m, 1H, NH); LRMS (ESI) [M^++Na] calcd for C$_{65}$H$_{82}$N$_4$O$_{12}$Na, 1061; found, 1061; elemental analysis calcd (%) for C$_{59}$H$_{82}$N$_4$O$_{12}$: C 68.18, H 7.95, N 5.39; found: C 67.99, H 7.90, N 5.30.

Compound **35** (85 mg, 82 μmol) was hydrolyzed in a similar manner as described above by using KOH to give the corresponding carboxylic acid **38** (see the Supporting Information) as a pale yellow amorphous solid (87 mg, 100%). m.p.: 168–172°C; ^{1}H NMR (400 MHz, [D$_6$]DMSO): δ = 1.14–1.30 (s, 29H, 3-, 4-, and 5-Boc and CH$_2$CH$_2$CH$_2$CO$_2$CH$_3$), 1.46–1.55

(m, 4H, -CH$_2$CH$_2$CO$_2$CH$_3$ and -CONHCH$_2$CH$_2$), 1.76–1.91 (m, 6H, 3-, 4-, and 5-OCH$_2$CH$_2$), 2.20 (t, *J* = 7.1 Hz, 2H, -CH$_2$CO$_2$CH$_3$), 2.67–2.73 (m, 6H, 3-, 4-, and 5-PhCH$_2$), 3.18–3.23 (m, 2H, -CONHCH$_2$), 3.84–3.99 (m, 9H, 3-, 4-, 5-OCH$_2$CH$_2$CH), 6.59 (d, *J* = 8.8 Hz, 1H, 4-NHBoc), 6.81 (d, *J* = 8.5 Hz, 1H, 3- and 5-NHBoc), 7.09–7.26 (m, 17H, 3,4,5-Ph and benzoyl) and 8.34 (m, 1H, benzoyl-CONH) and 11.9 ppm (br s, 1H, -CO$_2$H); HRMS–FAB (*m/z*): [M^++H] calcd for C$_{58}$H$_{81}$N$_4$O$_{12}$ [M^++H]: 1025.5851; found: 1025.5835.

PyBop (50 mg, 96 μmol) in CH$_2$Cl$_2$ (1 mL) was added to a solution of the free acid **38** (72 mg, 70 μmol), H-Cys(Trt)-Val-Ile-Leu-O*t*Bu (Trt = trityl; 66 mg, 89 μmol), HOBt (25 mg, 0.16 mmol), and DIEA (25 μL, 015 mmol) in DMF (6 mL) at 0°C. After stirring at room temperature for 17 h, concentration, extraction with CHCl$_3$, and purification by size-exclusion column chromatography (Sephadex LH-20, CHCl$_3$/MeOH = 1:1) gave the fully protected product (**41**; see the Supporting Information) as a white solid (86 mg, 70%). m.p.: 179–181°C; ^{1}H NMR (400 MHz, CDCl$_3$): δ = 0.68–0.86 (m, 18H, γ-CH$_3$ Val, γ-CH$_3$ Ile, δ-CH$_3$ Ile, and 2δ-CH$_3$ Leu), 0.97–1.04 (m, 1H, γ-CH Leu), 1.13–1.86 (m, 54H, γ-CH$_2$ Ile and β-CH$_2$ Leu, β-CH Ile, β-CH Val, 3-, 4-, and 5-OCH$_2$CH$_2$, -CONHCH$_2$(CH$_2$)$_3$, O*t*Bu and 3-, 4-, 5-Boc), 2.08 (m, 2H, β-CH$_2$, Cys), 2.33 (m, 2H, -CH$_2$CONH), 2.67–2.73 (m, 6H, 3-, 4-, and 5-CH$_2$Ph), 3.17 (m, 2H, -CONHCH$_2$), 3.84–3.98 (m, 9H, 3-, 4-, and 5-OCH$_2$CH$_2$CH), 4.12–4.27 (m, 4H, α-CH Cys, Val, Ieu, and Leu), 6.55 (d, *J* = 8.4 Hz, 4-NHBoc), 6.78 (d, *J* = 8.8 Hz, 2H, 3- and 5-NHBoc), 7.09–7.33 (m, 32H, aryl-H), 7.50 (d, *J* = 8.9 Hz, 1H, NH), 7.88 (d, *J* = 8.8 Hz, 1H, NH), 8.09 (d, *J* = 8.3 Hz, 1H, NH) 8.16 (d, *J* = 7.9 Hz, 1H, NH), 8.31 ppm (m, 1H, CONH); elemental analysis calcd (%) C$_{101}$H$_{138}$N$_8$O$_{16}$S·1.0H$_2$O: C 68.52, H 7.97, N 6.33; found: C 68.57, H 7.87, N 6.22; HRMS (*m/z*): [M^++H] calcd for C$_{101}$H$_{139}$N$_8$O$_{16}$S$_1$, 1752.003; found, 1752.0000.

This compound was deprotected by treatment with 50% TFA in CH$_2$Cl$_2$ in the presence of 5% triethylsilane at 0°C for 1 h. After concentration, the residue was suspended in Et$_2$O, sonicated, and centrifuged to collect the resulting white solid, which was washed with Et$_2$O several times, and dried to give **6**, a colorless white powder (21 mg, 100%). m.p.: 154–162°C; ^{1}H NMR (400 MHz, CDCl$_3$): δ = 0.78–0.86 (m, 18H, 2γ-CH$_3$ Val, γ-, δ-CH$_3$ Ile, and 2δ-CH$_3$ Leu), 1.02–1.11 (m, 1H, γ-CH Leu), 1.24–1.96 (m, 18H, 3,4,5-OCH$_2$CH$_2$, -CONHCH$_2$(CH$_2$)$_3$, β-CH Val, β-CH and γ-CH$_2$ Ile, and β-CH$_2$ Leu), 2.13–2.18 (m, 2H, -CH$_2$CONH), 2.62–2.78 (m, 2H, β-CH$_2$ Cys), 2.83–2.97 (m, 6H, 3,4,5-PhCH$_2$), 3.90–3.93 (m, 2H, α-CH×2), 4.09–4.20 (m, 7H, 3-, 4-, and 5-OCH$_2$ and α-CH), 4.40–4.45 (m, 1H, α-CH), 7.19–7.34 (m, 17H, 3-, 4-, and 5-Ph and benzoyl), 7.79–7.86 (m, 2H, -N*H*CH), 8.06–8.14 (m, 2H, -N*H*CH), 8.36–8.39 ppm (m, 1H, PhCONH); HRMS–FAB (*m/z*): [M^++H] calcd for C$_{69}$H$_{104}$N$_8$O$_{10}$S$_1$, 1153.6735; found, 1153.6702.

Protein expression and purification: The plasmids, GGTase I α subunit in pAlter-Ex2 (pAlter-Ex2-GGTα) and β subunit in pET28a (pET28a-GGTβ) were kindly provided by Prof. Casey from Duke University. The protein was expressed and purified as previously reported.[42,67] Briefly, the plasmids were successively transformed into BL21 (DE3) *E. coli* cells (Novagen), which grew until the optical density reached 0.6. GGTase I expression was induced by the addition of isopropyl-β-D-thiogalactoside (0.4 mM) and ZnSO$_4$ (0.5 mM), and the cells were harvested after 4 h and lysed. The soluble fraction of the cell lysate was bound to nickel agarose resin (Qiagen) by incubation for 1 h at 4°C in a buffer solution containing Tris-HCl (20 mM, pH 7.7), NaCl (300 mM), imidazole (5 mM), dithiothreitol (DTT; 1 mM), and protease inhibitor mix. The proteins were eluted with increasing concentrations of imidazole, and the appropriate fractions were immediately dialyzed and concentrated. The purity of the protein solution was checked by SDS-PAGE gels (> 90%).

General conditions for fluorescent enzyme assay: The inhibition activities of the synthetic compounds against GGTase I were measured by a kinetic assay by using the fluorogenic substrate, dansyl-Gly-Cys-Val-Ile-Leu (DansGCVIL), which was prepared by solid-phase peptide synthesis (see Figures S21 and S22 in the Supporting Information). The peptide buffer solution (53 mM Tris-HCl, pH 7.5, 0.1 mM ethylenediaminetetraacetate (EDTA), 0.020% *n*-dodecyl-β-D-maltoside, 5.0 mM DTT) was used for preparation of DansGCVIL stock solution, and the assay buffer solution (50 mM Tris-HCl, pH 7.50, 1.2 mM MgCl$_2$, 1.2 μM ZnCl$_2$, 0.023% *n*-dode-

cyl-β-D-maltoside, 5 mM DTT) was used for enzyme dilution and for running the kinetic assay. Commercially purchased GGPP ammonium salt methanol solution from Sigma–Aldrich was diluted with 25 mM NH$_4$HCO$_3$ to 500 mM and stored at −80°C in aliquots and further diluted to 110 μM before use (methanol content less than 5%). The peptide substrate, DansGCVIL, was dissolved in the peptide buffer solution (approximately 500 μM), and the concentration was determined from a standard curve of A_{340} versus the concentration of dansylglycine in the same buffer solution. Inhibitors were first dissolved in DMSO solution (1 or 30 mM) and further diluted with peptide buffer solution to various concentrations (1.1 μM to 2.2 mM), which were then used for the assay. The GGTase I solution (125 μM) was freshly diluted with the assay buffer solution prior to use (685 nM). The assays were performed at 30°C by using a thermostated curvette holder. Solutions of DansGCVIL (10 μL), GGPP (10 μL), and inhibitor (10 μL) were added to the assay buffer solution (180 μL) in a 500-μL tube, which was incubated in a 30°C water bath for 5 min. The GGTase I solution (10 μL) was added to this solution; the mixture was vortexed, quickly transferred to the cuvette, and the fluorescent intensity change at 520 nm (ex: 340 nm) was monitored for 5 min. The final concentrations of each component were; [DansGCVIL] = 1 μM, [GGPP] = 5 μM, [GGTase I] = 31 nM, [Inhibitors] = 0–100 μM (the content of DMSO in the final solution was less than 2%). The experiments for each concentration of inhibitor were repeated at least three times.

The raw data points were fit linearly and the resulting slopes were used to calculate IC$_{50}$ values, which were determined by plotting the data as percent inhibition versus the log of the concentration of the inhibitors used. The data were fit to the sigmoidal Equation (1) by using SigmaPlot (version 10, Systat software, Inc.).

$$y = a + \frac{(b-a)}{1 + 10^{(c-x)d}} \qquad (1)$$

In Equation (1), a and b are the minimal and maximal values of percentage of inhibition, x is the logarithm of the inhibitor concentration, c is the IC$_{50}$ value, and d is the Hill slope. The IC$_{50}$ values were further converted to the inhibition constant K_i values by using the Cheng–Prusoff equation (Equation (2)).[68]

$$K_i = \frac{IC_{50}}{1 + \left(\frac{[S]}{K_m}\right)} \qquad (2)$$

As shown in Equation (2), [S] is the substrate concentration and K_m ((0.28±0.04) μM) is the Michaelis constant of the substrate for the enzyme obtained from a Micahelis–Menten plot (see Figure S1 in the Supporting Information).

The Lineweaver–Burk analysis was carried out by using different substrate and inhibitor concentrations with a range of 0.1–1 μM and 0.1–5.0 μM, respectively. In all the cases, the GGPP concentration was fixed to 5 μM for the saturated condition. The Lineweaver–Burk plot of 1/v versus 1/[S] was analyzed by competitive, noncompetitive, and uncompetitive models with SigmaPlot and the best fit was obtained by a competitive model in which the initial velocity v is given by Equation (3).

$$v = \frac{V_{max}}{1 + \left(\frac{K_m}{[S]}\right)\left(1 + \frac{[I]}{K_i}\right)} \qquad (3)$$

In Equation (3), v is arbitrary fluorescence units per second, V_{max} is the maximum velocity of the reaction, and [I] is the inhibitor concentration.

In vitro GGTase I and FTase activity assays with [^{3}H]-labeled substrates: In vitro inhibition assays of mammalian FTase and GGTase I were performed by measuring the incorporation of [^{3}H] FPP (GE Healthcare, Piscataway, NJ) and [^{3}H] GGPP (Perkin-Elmer Life Sciences, Boston, MA) into wild-type H-Ras (FTase) and H-Ras-CVLL (GGTase I), respectively, as previously described.[71] Briefly, approximately 20μg of 60000×g postmicrosomal supernatant from SF-9 cells expressing human GGTase I or FTase was incubated in the presence of an increasing concentration of

compound, 10 μg H-Ras or H-Ras-CVLL substrate, and 0.5 μCi/sample of either [^{3}H] FPP or [^{3}H] GGPP. Samples were precipitated by using tricarboxylic acid (TCA) and then filtered onto glass-fiber filters; unbound [^{3}H] FPP or [^{3}H] GGPP was washed through the filters. Samples were counted in a scintillation counter and the activity was compared with vehicle controls to obtain IC$_{50}$ values.

[1] P. Bork, L. J. Jensen, C. V. Merg, A. K. Ramani, I. Lee, E. M. Marcotte, *Curr. Opin. Struct. Biol.* **2004**, *14*, 292–299.

[2] B. P. Orner, J. T. Ernst, A. D. Hamilton, *J. Am. Chem. Soc.* **2001**, *123*, 5382–5383.

[3] S. Fletcher, A. D. Hamilton, *Curr. Opin. Chem. Biol.* **2005**, *9*, 632–638.

[4] H. Yin, A. D. Hamilton, *Angew. Chem.* **2005**, *117*, 4200–4235; *Angew. Chem. Int. Ed.* **2005**, *44*, 4130–4163.

[5] L. Pagliaro, J. Felding, K. Audouze, S. J. Nielsen, R. B. Terry, C. Krog-Jensen, S. Bucher, *Curr. Opin. Chem. Biol.* **2004**, *8*, 442–449.

[6] M. R. Arkin, J. A. Wells, *Nat. Rev. Drug Discovery* **2004**, *3*, 301–317.

[7] J. A. Kritzer, R. Zutshi, M. Cheah, F. A. Ran, R. Webman, T. M. Wongjirad, A. Schepartz, *ChemBioChem* **2006**, *7*, 29–31.

[8] S. E. Rutledge, H. M. Volkman, A. Schepartz, *J. Am. Chem. Soc.* **2003**, *125*, 14336–14347.

[9] S. Rajagopal, S. C. Meyer, A. Goldman, M. Zhou, I. Ghosh, *J. Am. Chem. Soc.* **2006**, *128*, 14356–14363.

[10] T. J. Smith, C. I. Stains, S. C. Meyer, I. Ghosh, *J. Am. Chem. Soc.* **2006**, *128*, 14456–14457.

[11] R. L. A. Dias, R. Fasan, K. Moehle, A. Renard, D. Obrecht, J. A. Robinson, *J. Am. Chem. Soc.* **2006**, *128*, 2726–2732.

[12] Y. Hamuro, M. Calama, H. Park, A. D. Hamilton, *Angew. Chem.* **1997**, *109*, 2797–2800; *Angew. Chem. Int. Ed.* **1997**, *36*, 2680–2683.

[13] H. S. Park, Q. Lin, A. D. Hamilton, *Proc. Natl. Acad. Sci. USA* **2002**, *99*, 5105–5109.

[14] H. C. Zhou, L. Baldini, J. Hong, A. J. Wilson, A. D. Hamilton, *J. Am. Chem. Soc.* **2006**, *128*, 2421–2425.

[15] K. Groves, A. J. Wilson, A. D. Hamilton, *J. Am. Chem. Soc.* **2004**, *126*, 12833–12842.

[16] R. K. Jain, A. D. Hamilton, *Org. Lett.* **2000**, *2*, 1721–1723.

[17] J. E. Gestwicki, G. R. Crabtree, I. A. Graef, *Science* **2004**, *306*, 865–869.

[18] S. L. Hussey, S. S. Muddana, B. R. Peterson, *J. Am. Chem. Soc.* **2003**, *125*, 3692–3693.

[19] D. A. Erlanson, J. W. Lam, C. Wiesmann, T. N. Luong, R. L. Simmons, W. L. Delano, I. C. Choong, M. T. Burdett, W. M. Flanagan, D. Lee, E. M. Gordon, T. O'Brien, *Nat. Biotechnol.* **2003**, *21*, 308–314.

[20] Y. Takaoka, H. Tsutsumi, N. Kasagi, E. Nakata, I. Hamachi, *J. Am. Chem. Soc.* **2006**, *128*, 3273–3280.

[21] J. Dimaio, B. Gibbs, D. Munn, J. Lefebvre, F. Ni, Y. Konishi, *J. Biol. Chem.* **1990**, *265*, 21698–21703.

[22] T. Steinmetzer, B. Y. Zhu, Y. Konishi, *J. Med. Chem.* **1999**, *42*, 3109–3115.

[23] K. M. Jude, A. L. Banerjee, M. K. Haldar, S. Manokaran, B. Roy, S. Mallik, D. K. Srivastava, D. W. Christianson, *J. Am. Chem. Soc.* **2006**, *128*, 3011–3018.

[24] A. L. Banerjee, M. Swanson, B. C. Roy, X. Jia, M. K. Haldar, S. Mallik, D. K. Srivastava, *J. Am. Chem. Soc.* **2004**, *126*, 10875–10883.

[25] K. Enander, G. T. Dolphin, L. Baltzer, *J. Am. Chem. Soc.* **2004**, *126*, 4464–4465.

[26] B. A. Grzybowski, A. V. Ishchenko, C. Y. Kim, G. Topalov, R. Chapman, D. W. Christanson, G. M. Whitesides, E. I. Shakhnovich, *Proc. Natl. Acad. Sci. USA* **2002**, *99*, 1270–1273.

[27] P. A. Boriack, D. W. Christianson, J. Kingery-Wood, G. M. Whitesides, *J. Med. Chem.* **1995**, *38*, 2286–2291.

[28] N. Schaschke, D. Gabrijelcic-Geiger, A. Dominik, C. P. Sommerhoff, *ChemBioChem* **2005**, *6*, 95–103.

[29] K. Shen, P. A. Cole, *J. Am. Chem. Soc.* **2003**, *125*, 16172–16173.

[30] A. Profit, A. T. R. Lee, D. S. Lawrence, *J. Am. Chem. Soc.* **1999**, *121*, 280–283.

[31] B. C. Roy, A. L. Banerjee, M. Swanson, X. G. Jia, M. K. Haldar, S. Mallik, D. K. Srivastava, *J. Am. Chem. Soc.* **2004**, *126*, 13206–13207.

[32] M. C. Seabra, Y. Reiss, P. J. Casey, M. S. Brown, *Cell* **1991**, *65*, 429–434.

[33] W. W. Epstein, D. Lever, L. M. Leining, E. Bruenger, H. C. Rilling, *Proc. Natl. Acad. Sci. USA* **1991**, *88*, 9668–9670.

[34] P. J. Casey, *J. Lipid Res.* **1992**, *33*, 1731–1740.

[35] K. Zhu, A. D. Hamilton, S. M. Sebti, *Curr. Opin. Invest. Drugs* **2003**, *4*, 1428–1435.

[36] F. G. Njoroge, A. G. Taveras, J. Kelly, S. Remiszewski, A. K. Mallams, R. Wolin, A. Afonso, A. B. Cooper, D. F. Rane, Y. T. Liu, J. Wong, B. Vibulbhan, P. Pinto, J. Deskus, C. S. Alvarez, J. D. Rosario, M. Connolly, J. Wang, J. Desai, R. R. Rossman, W. R. Bishop, R. Patton, L. Wang, P. Kirschmeier, M. S. Bryant, A. A. Nomeir, C. C. Lin, M. Liu A. T. McPhail, R. J. Doll, V. M. Girijavallabhan, A. K. Ganguly, *J. Med. Chem.* **1998**, *41*, 4890–4902.

[37] L. Wang, G. T. Wang, X. Wang, Y. Tong, G. Sullivan, D. Park, N. M. Leonard, Q. Li, J. Cohen, W. Gu, H. Zhang, J. L. Bauch, C. G. Jakob, C. W. Hutchins, V. S. Stoll, K. Marsh, S. H. Rosenberg, H. L. Sham, N. Lin, *J. Med. Chem.* **2004**, *47*, 612–626.

[38] A. D. Basso, P. Kirschmeier, W. R. Bishop, *J. Lipid Res.* **2006**, *47*, 15–31.

[39] M. H. Gelb, L. Brunsveld, C. A. Hrycyna, S. Michaelis, F. Tamanoi, W. C. V. Boorhis, H. Waldmann, *Nat. Chem. Biol.* **2006**, *2*, 518–528.

[40] M. R. Philips, A. D. Cox, *J. Clin. Invest.* **2007**, *117*, 1223–1225.

[41] J. Sun, J. Ohkanda, D. Coppola, H. Yin, M. Kothare, B. Busciglio, A. D. Hamilton, S. M. Sebti, *Cancer Res.* **2003**, *63*, 8922–8929.

[42] Y. K. Peterson, P. Kelly, C. A. Weinbaum, P. J. Casey, *J. Biol. Chem.* **2006**, *281*, 12445–12450.

[43] H. Peng, D. Carrico, V. Thai, M. A. Blaskovich, C. Bucher, E. E. Pusateri, S. M. Sebti, A. D. Hamilton, *Org. Biomol. Chem.* **2006**, *4*, 1768–1784.

[44] A. M. Sjogren, K. M. Andersson, M. Liu, B. A. Cutts, C. Karlsson, A. M. Wahlstrom, M. Dalin, C. Weinbaum, P. J. Casey, A. Tarkowski, B. Swolin, S. G. Young, M. O. Bergo, *J. Clin. Invest.* **2007**, *117*, 1294–1304.

[45] S. Castellano, H. D. G. Fiji, S. S. Kinderman, M. Watanabe, P. D. Leon, F. Tamanoi, O. Kwon, *J. Am. Chem. Soc.* **2007**, *129*, 5843–5845.

[46] B. S. Zuckerbraun, J. E. Barbato, A. Hamilton, S. Sebti, E. Tzeng, *J. Surg. Res.* **2005**, *124*, 256–263.

[47] J. Ye, C. Wang, J. Rhea Sumpter, M. S. Brown, J. L. Goldstein, J. Michael Gale, *Proc. Natl. Acad. Sci. USA* **2003**, *100*, 15865–15870.

[48] R. Khosravi-Far, P. A. Solski, G. J. Clark, M. S. Kinch, C. J. Der, *Mol. Cell. Biol.* **1995**, *15*, 6443–6453.

[49] E. A. Clark, T. R. Golub, E. S. Lander, R. O. Hynes, *Nature* **2000**, *406*, 532–535.

[50] P. L. Joyce, A. D. Cox, *Cancer Res.* **2003**, *63*, 7959–7967.

[51] R. G. Qiu, A. Abo, F. McCormick, M. Symons, *Mol. Cell. Biol.* **1997**, *17*, 3449–3458.

[52] K. Lim, A. T. Baines, J. J. Fiordalisi, M. Shipitsin, L. A. Feig, A. D. Cox, C. J. Der, C. M. Counter, *Cancer Cell* **2005**, *7*, 533–545.

[53] E. C. Lerner, Y. M. Qian, A. D. Hamilton, S. M. Sebti, *J. Biol. Chem.* **1995**, *270*, 26770–26773.

[54] D. B. Whyte, P. Kirschmeier, T. N. Hockenberry, I. Nunez-Oliva, L. James, J. J. Catino, W. R. Bishop, J. Pai, *J. Biol. Chem.* **1997**, *272*, 14459–14464.

[55] C. A. Rowell, J. J. Kowalczyk, M. D. Lewis, A. M. Garcia, *J. Biol. Chem.* **1997**, *272*, 14093–14097.

[56] K. L. Terry, P. J. Casey, L. S. Beese, *Biochemistry* **2006**, *45*, 9746–9755.

[57] T. S. Reid, S. B. Long, L. S. Beese, *Biochemistry* **2004**, *43*, 9000–9008.

[58] J. S. Taylor, T. S. Reid, K. L. Terry, P. J. Casey, L. S. Beese, *EMBO J.* **2003**, *22*, 5963–5974.

[59] G. L. James, J. L. Goldstein, M. S. Brown, *J. Biol. Chem.* **1995**, *270*, 6221–6226.

[60] F. L. Zhang, P. Kirschmeier, D. Carr, L. James, R. W. Bond, L. Wang, R. Patton, W. Windsor, R. Syto, R. Zhang, W. R. Bishp, *J. Biol. Chem.* **1997**, *272*, 10232–10239.

[61] S. B. Long, P. J. Casey, L. S. Beese, *Structure* **2000**, *8*, 209–222.

[62] I. Smalera, J. M. Williamson, W. Baginsky, M. Leiting, P. Mazur, *Biochim. Biophys. Acta* **2000**, *1480*, 132–144.

[63] K. T. Lane, L. S. Beese, *J. Lipid Res.* **2006**, *47*, 681–699.

[64] T. S. Reid, K. L. Terry, P. J. Casey, L. S. Beese, *J. Mol. Biol.* **2004**, *343*, 417–433.

[65] S. L. Moores, M. D. Schaber, S. D. Mosser, E. Rands, M. B. O'Hara, V. M. Garsky, M. S. Marshall, D. L. Pompliano, J. B. Gibbs, *J. Biol. Chem.* **1991**, *266*, 14603–14610.

[66] W. G. Stirtan, C. D. Poulter, *Biochemistry* **1997**, *36*, 4552–4557.

[67] H. Fu, J. F. Moomaw, C. R. Moomaw, P. J. Casey, *J. Biol. Chem.* **1996**, *271*, 28541–28548.

[68] Y. Cheng, W. H. Prusoff, *Biochem. Pharmacol.* **1973**, *22*, 3099–3108.

[69] D. K. Srivastava, K. M. Jude, A. L. Banerjee, M. Haldar, S. Manokaran, J. Kooren, S. Mallik, D. W. Christianson, *J. Am. Chem. Soc.* **2007**, *129*, 5528–5537.

[70] P. Broto, G. Moreau, C. Vandycke, *Eur. J. Med. Chem.* **1984**, *19*, 71–78.

[71] A. Vogt, Y. Qian, T. F. McGuire, A. D. Hamilton, S. M. Sebti, *Oncogene* **1996**, *13*, 1991–1999.

[72] S. B. Long, P. J. Hancock, A. M. Kral, H. W. Hellinga, L. S. Beese, *Proc. Natl. Acad. Sci. USA* **2001**, *98*, 12948–12953.